

# Online Impedance Adaptation Facilitates Manipulating a Whip

Xiaofeng Xiong<sup>1</sup>, Moses C. Nah<sup>2</sup>, Aleksei Krotov<sup>3</sup> and Dagmar Sternad<sup>4</sup>

**Abstract**—Flexible object manipulation is one of the major challenges in robotics. The complex and nonlinear dynamics originating from the high dimensional object structure makes it difficult to apply state-of-the-art methods. Dynamic primitives-based approach has been shown to bypass the need of a detailed object model and instead optimized a small set of movement parameters that achieved the task. However, most of the studies have mainly focused on optimization of motion primitives, leaving the interactive primitives aside.

To account for the interactive dynamics between the controller and the manipulated object, we extended the previous method by adding online impedance adaptation (OIA) controller that modulated the joint impedances in real-time. We demonstrated the effectiveness of this extension by simulating a task of hitting a target with a whip manipulated by a two-joint manipulator. Including the OIA control law led to faster optimization of the targeting task and smaller deviation of joints from zero-torque trajectories, compared to the controller with constant joint impedances. This novel way to control both motion and impedance of a manipulator as a whole may provide means to facilitate manipulation of objects with significant dynamics.

## I. INTRODUCTION

A prominent challenge in the field of robotics is manipulation of flexible objects [1]. The complex and nonlinear dynamics originating from the high (in principle, an infinite) dimensional structure makes it difficult to apply state-of-the-art methods, which are mostly focused on rigid object manipulation [2]. Several attempts were made to simplify the problem — an exemplary way is to reduce the number of its degree-of-freedom (DOF) to a finite lumped-parameter model and apply popular optimization based approaches. However, due to the “curse of dimensionality”, the computational complexity of the task grows exponentially with system dimension, and the optimization quickly becomes intractable [3].

Recent studies in human motor control demonstrated that composing a controller based on motor primitives provided

<sup>1</sup>Xiaofeng Xiong is with SDU Biorobotics, the Mærsk Mc-Kinney Møller Institute, the University of Southern Denmark (SDU), Odense, Denmark, supported by the Human Frontier Science Program, Grant no. RGP 0002/2017. [xizi@mmti.sdu.dk](mailto:xizi@mmti.sdu.dk)

<sup>2</sup>Moses C. Nah is with the Department of Mechanical Engineering, Massachusetts Institute of Technology, Cambridge, MA, USA, supported in part by NSF M3X-1826097 (Neville Hogan) and NIH-R01-HD087089. [mosesnah@mit.edu](mailto:mosesnah@mit.edu)

<sup>3</sup>Aleksei Krotov is with the Department of Bioengineering, Northeastern University, Boston, MA, USA, supported in part by NSF M3X-1825942 (Dagmar Sternad) and Fulbright-IIE-PS00261102. [krotov.a@northeastern.edu](mailto:krotov.a@northeastern.edu)

<sup>4</sup>Dagmar Sternad is with the Departments of Biology, Electrical and Computer Engineering, and Physics, Northeastern University, Boston, MA, USA, supported in part by NSF M3X-1825942 and NIH-R01-HD087089. [d.sternad@northeastern.edu](mailto:d.sternad@northeastern.edu)

a way to simpler solutions for complex object manipulation [4]–[10]. Nah et al. developed a controller composed of dynamic motor primitives to manipulate one of the most complex and exotic tools which humans can manipulate – a whip [11]–[13]. The study tested in simulation whether a distant target could be reached with a whip controlled by a 2-DOF manipulator using a controller composed of primitive actions. It was discovered that without the need of a precise and detailed model of the whip dynamics, the offline optimization was able to identify an optimal submovement in joint space coordinates that achieved the targeting task. This approach provided a way to work around the curse of dimensionality and highlighted the benefits of primitive actions for manipulating complex objects.

While the primitives-based approaches demonstrated effective means for complex object manipulation, most studies have focused on optimization of motion primitives, leaving the interactive primitives aside. In particular, Nah et al. assumed constant joint impedances and only optimized the movement parameters of the controller [11]. Studies in both robotics, human-robot interaction [14]–[16] and human motor control [17]–[20] emphasized the crucial role of mechanical impedance in physical interaction. For example, Averta et al. simulated time-varying joint impedances for a 14-DOF Baxter Robot, to enable a smooth transition from free motion to a contact [14]. Bitz et al. reported variable and negative damping in a 7-DOF manipulator in a 3-D reaching task, that led to improved movement accuracy and reduced effort [16]. Huang et al. demonstrated improved motor performance in humans after force-field training with negative viscosity [20]. Following these lines of studies, a controller which adaptively modulates mechanical impedance may improve task performance and the efficiency of optimization.

In this paper, we extended the work done in [11] by replacing the constant impedance with an online impedance adaptation (OIA) controller [21]. In addition to optimizing the 5 parameters of a single submovement, the joint impedances of the upper-limb were modulated online (i.e., real-time) to reach a distant target with a whip. This extension was tested in three high-DOF (i.e., 10, 15, 25) whip models, manipulated by a two-joint arm model. The results demonstrated that augmenting the previous controller with an OIA control law leads to faster task optimization and smaller joint position tracking errors [11]. As our approach provides a novel way to plan the motion and impedance of a manipulator as a whole, we assume that this method may provide a mean to facilitate manipulating objects with significant dynamics.

## II. METHODS

The research presented in this paper used the simulation software MuJoCo [22]. The semi-implicit Euler method was chosen as the numerical integrator with a time step of 0.1 ms.

### A. Modeling

A two-joint human upper-limb model (the manipulator) and an  $N$ -node whip model (the manipulated object) were used for the simulation. The planar 2-DOF upper-limb robot, developed in Nah et al. [11], was used for the manipulator, where the geometrical and inertial parameters were borrowed from Hatze [23]. Independently controlled torque actuators were mounted co-axially on both joints.

The continuous dynamics of the whip was discretized to an  $N$ -node lumped-parameter model. A single sub-model of the whip comprised of an (ideal) point-mass and a compliant rotational pivot. A point-mass  $m$  [kg], was suspended from a massless cylinder with length  $l$  [m], and the compliant pivot consisted of a linear rotational spring and linear rotational damper with coefficient  $k$  [N·m/rad] and  $b$  [N·m·s/rad], respectively [11], [12].  $N$  of these sub-models were serially connected in a chain-like manner, which resulted in an  $N$ -node whip model. The parameters ( $N$ ,  $l$ ,  $m$ ,  $k$ ,  $b$ ) will be called the “whip parameters” of the  $N$ -node whip model. Three whip models were constructed (Table I): the short, medium and long whip model, where the parameters of the latter one were experimentally identified from an actual bullwhip [11], [24].<sup>1</sup>

TABLE I: The model parameters of the whip

	Whip Parameters				
	$N$	$l$	$m$	$k$	$b$
Short whip	10	0.1	0.1	0.050	0.005
Medium whip	15	0.1	0.1	0.050	0.005
Long whip	25	0.072	0.012	0.242	0.092

The connection between the upper-limb and whip was achieved with a freely-rotating hinge joint, i.e., no stiffness or damping elements were included for the handle. Summarizing, the combined model resulted in a sequential open-chain planar mechanism with  $(N + 2)$ -DOF.

### B. The Upper-limb Controller

1) *Impedance Controller*: First order impedance controller with gravity compensation was used for the 2-DOF upper-limb model:

$$\tau = \mathbf{K}(\mathbf{q}_d - \mathbf{q}) + \mathbf{B}(\dot{\mathbf{q}}_d - \dot{\mathbf{q}}) + \boldsymbol{\tau}_G \quad (1)$$

where torque  $\boldsymbol{\tau}_G(t) \in \mathbb{R}^2$  denotes the torque required for gravity compensation (Sec. II-B.2);  $\mathbf{q}(t) \in \mathbb{R}^2$  denotes the actual joint angle trajectory of the upper-limb, defined in

<sup>1</sup>The experimentally-fitted whip model constructed in [11] corresponds to the long whip model of this report

relative angle coordinates;  $\mathbf{q}_d(t) \in \mathbb{R}^2$  denotes the “zero-torque” trajectory, i.e., neglecting gravitational effects, when the actual joint trajectory,  $\mathbf{q}$  exactly matches with zero-torque trajectory,  $\mathbf{q}_d$ , then zero torque will be exerted by the joint actuators (Sec. II-B.3);  $\mathbf{K}(t) \in \mathbb{R}^{2 \times 2}$  and  $\mathbf{B}(t) \in \mathbb{R}^{2 \times 2}$  are the time-varying stiffness and damping matrices representing the neuromuscular mechanical impedance of the upper-limb, respectively; the impedance matrices  $\mathbf{K}(t)$  and  $\mathbf{B}(t)$  are online adapted via OIA control law (Sec. II-B.4);

2) *Gravity Compensation*: Gravitational effects due to the mass of the upper-limb and the whip model were compensated with  $\boldsymbol{\tau}_G(t)$ , such that the actual upper-limb posture,  $\mathbf{q}$  could exactly match with the zero-torque posture,  $\mathbf{q}_d$ , when the whole model was at rest. In detail [12]:

$$\boldsymbol{\tau}_G = \mathbf{J}_1^T \mathbf{f}_1 + \mathbf{J}_2^T \mathbf{f}_2 + \mathbf{J}_3^T \mathbf{f}_3 \quad (2)$$

where  $\mathbf{J}_{1-3} \in \mathbb{R}^{3 \times 2}$  are the Jacobian matrices in terms of the center of mass of the upperarm, center of mass of the forearm, and the end-effector with respect to the frame attached to the shoulder, respectively.

$\mathbf{f}_{1-3} \in \mathbb{R}^3$  denote the gravitational forces due to the mass of the upperarm, forearm, and whip model, respectively [12]:

$$\mathbf{f}_1 = M_1 \mathbf{g}, \quad \mathbf{f}_2 = M_2 \mathbf{g}, \quad \mathbf{f}_3 = M_w \mathbf{g} \quad (3)$$

where  $M_1 = 0.291\text{kg}$  and  $M_2 = 0.294\text{kg}$  denote the mass of upper arm and forearm, respectively [11];  $M_w$  denotes the total mass of the whip model, which is the node number of the whip,  $N$  times the mass of a single sub-model,  $m$  ( $M_w = N \cdot m$ );  $\mathbf{g} \in \mathbb{R}^3$  denotes gravity in the simulation environment.

3) *Zero-torque Trajectory*: The zero-torque trajectory of the controller,  $\mathbf{q}_d(t)$  (Eq. 1) followed a minimum-jerk trajectory [25]:

$$\mathbf{q}_d(t) = \mathbf{q}_i + (\mathbf{q}_f - \mathbf{q}_i) \left\{ 10\left(\frac{t}{D}\right)^3 - 15\left(\frac{t}{D}\right)^4 + 6\left(\frac{t}{D}\right)^5 \right\} \quad (4)$$

where  $\mathbf{q}_i = [q_{i,s}, q_{i,e}]^T$  [rad] and  $\mathbf{q}_f = [q_{f,s}, q_{f,e}]^T$  [rad] denote the initial and final joint posture, respectively;  $D$  [s] is the duration of zero-torque trajectory; subscripts  $s$  and  $e$  denote shoulder and elbow joint, respectively; For times greater than the duration  $D$  (i.e.  $t > D$ ), the zero-torque trajectory,  $\mathbf{q}_d(t)$  remained at  $\mathbf{q}_f$ .

4) *Online Impedance Adaptation (OIA)*: The elements of the joint stiffness matrix  $\mathbf{K}(t)$  and damping matrix  $\mathbf{B}(t)$  of the impedance controller were online adapted:

$$\mathbf{K}(t) = \begin{bmatrix} k_{ss}(t) & k_{se}(t) \\ k_{es}(t) & k_{ee}(t) \end{bmatrix}, \quad \mathbf{B}(t) = \begin{bmatrix} b_{ss}(t) & b_{se}(t) \\ b_{es}(t) & b_{ee}(t) \end{bmatrix} \quad (5)$$

where  $k(t)$  and  $b(t)$  are the muscular stiffness and damping parameters of the upper-limb model [26]; subscript  $s$  and  $e$  correspond to the shoulder and elbow joint, respectively; diagonal and off-diagonal terms correspond to the impedances arising from the monoarticular and biarticular muscles of the upper-limb, respectively (Fig. 1).

The adaptation law of the impedance matrices  $\mathbf{K}(t)$  and  $\mathbf{B}(t)$  minimized the following scalar cost function  $J$ :

$$J = J_c + J_p \quad (6)$$

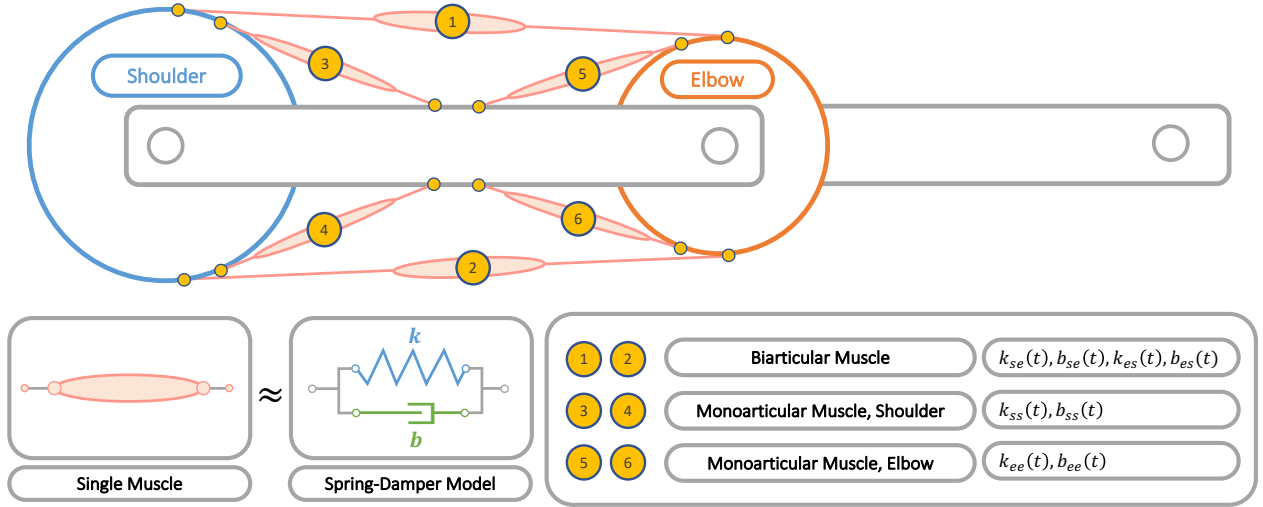


Fig. 1: A muscular model of the two-joint upper-limb used for the simulation. The monoarticular and biarticular muscles of the shoulder and elbow joints are depicted.

The cost function  $J_c$  is defined as follows:

$$J_c = \frac{1}{2} \int_0^D \left( \|\text{vec}(\tilde{\mathbf{K}})\|_{\mathbf{Q}_K}^2 + \|\text{vec}(\tilde{\mathbf{B}})\|_{\mathbf{Q}_B}^2 \right) d\tau \quad (7)$$

which is the time integration of the weighted norms of matrices  $\tilde{\mathbf{K}}, \tilde{\mathbf{B}} \in \mathbb{R}^{2 \times 2}$  from the start to the end of zero-torque trajectory (Eq. 4);  $\|\cdot\|_{\mathbf{Q}_K, \mathbf{Q}_B}$  and  $\text{vec}(\cdot)$  denote the weighted norms and column vectorization, respectively;  $\mathbf{Q}_K \in \mathbb{R}^{4 \times 4}$  and  $\mathbf{Q}_B \in \mathbb{R}^{4 \times 4}$  are positive symmetric weighting matrices where the norm of the matrix affects the speed of optimization [21];  $\tilde{\mathbf{K}}$  and  $\tilde{\mathbf{B}}$  are defined as the difference between the actual and expected values of the stiffness and damping matrices [21]:

$$\tilde{\mathbf{K}} = \mathbf{K} - \mathbf{K}_E, \quad \tilde{\mathbf{B}} = \mathbf{B} - \mathbf{B}_E \quad (8)$$

where subscript  $E$  denotes the expected impedance (matrices) for achieving stability.

The cost function  $J_p$  is defined as follows:

$$J_p = \int_0^D \dot{V}(\tau) d\tau, \quad V(t) = \frac{1}{2} \boldsymbol{\varepsilon}^T(t) \mathbf{I}(\mathbf{q}) \boldsymbol{\varepsilon}(t) \quad (9)$$

where the integrand is the time differentiation of scalar function  $V(t)$ , integrated from start to end of zero-torque trajectory (Eq. 4);  $\mathbf{I}(\mathbf{q}) \in \mathbb{R}^{2 \times 2}$  is the inertia matrix of the 2-DOF upper-limb model;  $\boldsymbol{\varepsilon}(t)$  is the time-varying sliding variable [27], defined as follows:

$$\boldsymbol{\varepsilon}(t) = \mathbf{e}(t) + \beta \dot{\mathbf{e}}(t), \quad \mathbf{e}(t) = \mathbf{q}_d(t) - \mathbf{q}(t) \quad (10)$$

where  $\mathbf{e}(t) \in \mathbb{R}^2$  is the tracking error between the zero-torque trajectory and the actual joint trajectory of the upper-limb model;  $\beta$  is a positive constant.

The resulting adaptation law of the impedances which minimized the cost function  $J$  is as follows [21]:

$$\mathbf{K}(t) = \mathbf{F}(t) \mathbf{e}^T(t), \quad \mathbf{B}(t) = \mathbf{F}(t) \dot{\mathbf{e}}^T(t), \quad \mathbf{F}(t) = \frac{\boldsymbol{\varepsilon}(t)}{\gamma(t)} \quad (11)$$

where  $\gamma(t)$  is an adaptation scalar defined as:

$$\gamma(t) = \frac{a}{1 + C \|\boldsymbol{\varepsilon}(t)\|^2}. \quad (12)$$

The values of the positive scalars used for the simulation are  $a = 0.2$  and  $C = 5$ . They are chosen for online stable adaptation control. Further details and stability proof of the online impedance adaptation law (Eq. 11) were presented in [21].

### C. Task Definition and Optimization

A whip task was defined to evaluate the performance of the upper-limb movement guided by the suggested controller. The task objective was to hit a distant target with a whip (Fig. 2). That objective was quantified as minimizing the distance between the tip of the whip and target,  $L$  [m]. The target was located at the shoulder height and 0.01m beyond the whip range [11]. Three whip models — the short, medium and long whip model (Sec. II-A and Table I) — were tested.

For the ZTTO controller, submovement parameters of a zero-torque trajectory,  $(q_{i,s}, q_{i,e}, q_{f,s}, q_{f,e}, D)$  (Eq. 4), were optimized using the global derivative-free optimization algorithm DIRECT-L (DIviding RECTangles Locally biased) under the nlopt (nonlinear optimization) Python tool box [28]. For the ZTTO + OIA controller, after each iteration of the submovement optimization, joint impedances were additionally modulated in real-time. The optimization was terminated when the distance  $L$  was lower than the threshold value  $L_d = 0.10\text{m}$ , i.e.,  $\text{Min}(L^*) < L_d$  (**Algorithm 1**). The obtained minimal distance,  $L^*$  [m], determined the performance.

## III. EXPERIMENTS AND RESULTS

To demonstrate the effectiveness of the OIA control law, it was compared to the controller with constant joint impedance parameters [11] (Eq. 13, see the experimental video<sup>2</sup>). Both

<sup>2</sup>[https://www.youtube.com/watch?v=AV\\_7qP6Yd-Y](https://www.youtube.com/watch?v=AV_7qP6Yd-Y)

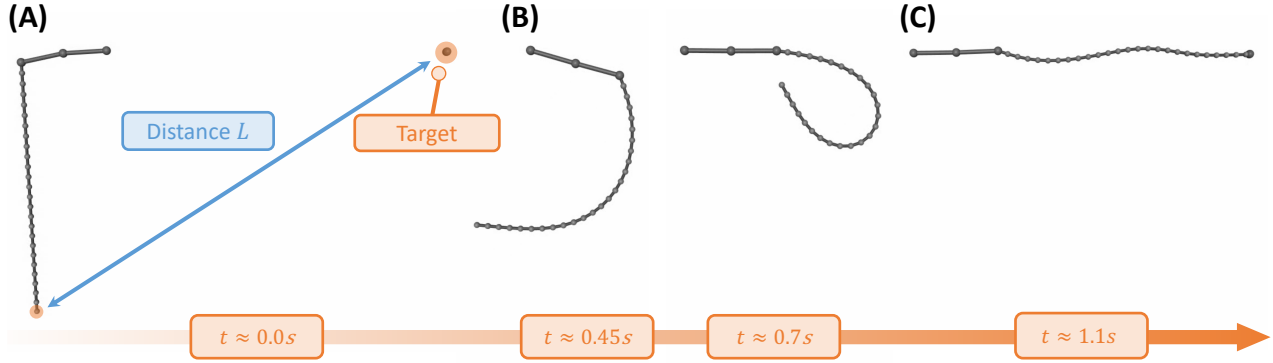


Fig. 2: Time sequence of the simulation using the long whip model (see Table I). (A) the beginning of the movement, (B) the intermediate movement phase and the final arm posture, (C) the whip reaching the minimal distance to the target.

---

**Algorithm 1:** Optimization of the whip task

---

**Inputs:**  $L_d = 0.10\text{m}$  (threshold distance);  
**Outputs:** Optimal  $(q_{i,s}, q_{i,e}, q_{f,s}, q_{f,e}, D)$  (Eq. 4);  
 Optimization initialization,  $t_0 = 0.05\text{s}$ ,  $T = 1.2\text{s}$ ;  
**for**  $\text{DIRECT-}L$ ,  $i = 1$  to  $600$  **do**  
 Simulation initialization;  
 Update  $(q_{i,s}, q_{i,e}, q_{f,s}, q_{f,e}, D)$  (Eq. 4);  
**while**  $0 \leq t < T$  **do**  
 Compute  $\tau_G$  (Eq. 2);  
**while**  $t_0 \leq t < t_0 + D$  **do**  
 Compute  $q_d, \dot{q}_d, e, \dot{e}$  (Eq. 4 and 10);  
**if**  $OIA == True$  **then**  
 | Update  $K$  and  $B$  (Eq. 11);  
**else**  
 | Use constant  $K$  and  $B$  (Eq. 13);  
**end**  
**end**  
 Compute/command torque inputs  $\tau$  (Eq. 1);  
 Compute and save distance  $L$ ;  
**end**  
 Save  $L^* = \text{Min}(L)$ ;  
**if**  $\text{Min}(L^*) < L_d$  **then**  
 | break;  
**end**  
**end**  
 Save the performance  $\text{Min}(L^*)$  and movement parameters  $[q_{i,s}, q_{i,e}, q_{f,s}, q_{f,e}, D]^T$ ;

---

controllers performed optimization of the whip task (Sec. II-C). Throughout this paper, the controller with constant impedance parameters is referred to as “ZTTO” (zero-torque trajectory optimization) controller, and the controller which additionally used the online impedance adaption (OIA) law is referred to as “ZTTO + OIA” controller.

For all three whip models, the proposed ZTTO + OIA approach outperformed the ZTTO approach in the following aspects:

1) *Faster Task Optimization:* The threshold value  $L_d = 0.10\text{m}$  was reached in fewer iterations with the ZTTO + OIA

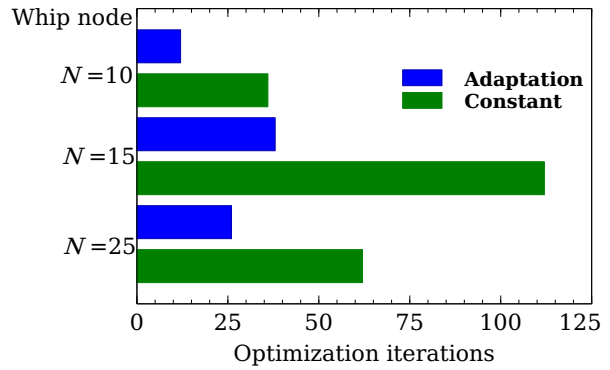


Fig. 3: Number of iterations before reaching the threshold distance between the whip and the target  $L_d = 0.1\text{m}$ . ZTTO controller assumed constant impedances, while ZTTO + OIA controller adapted and modulated impedances

controller, compared to the ZTTO controller, roughly by a factor of 2 (Fig. 3).

2) *Smaller Joint Position Tracking Errors:* The tracking errors of joint position were smaller for the ZTTO + OIA controller, indicating better tracking of the zero-torque trajectory (Fig. 4C, 4E).

#### IV. DISCUSSION AND CONCLUSION

The approach presented in this paper provided a novel way of planning both motion and impedance of a manipulator to manipulate a whip — one of the most complex and exotic tools which humans can handle. Not only did the controller optimize the parameters of the motion primitives (ZTTO), but an adaptation law modulated the mechanical impedances in real-time (OIA) (Fig. 5). Adding the OIA controller accounted for the physical interaction with the whip and led to faster optimization of the targeting task and smaller joint tracking errors, compared to the ZTTO controller with constant joint impedances.

The ZTTO + OIA controller resulted in time-varying mechanical impedances of the upper-limb model (Fig. 5). Stiffness increased during the early arm movement (from 0s to 0.45s), rapidly dropped to negative values, then converged

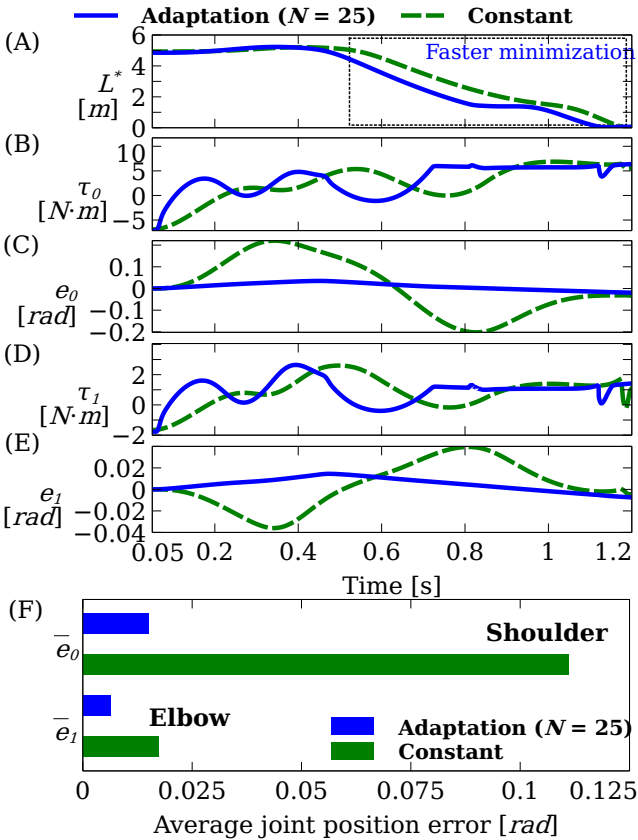


Fig. 4: Task-specific parameters during execution using the long whip model, with the ZTTO (green dashed line) and ZTTO + OIA (blue line) controllers. (A) Distance  $L$  between the whip and target. (B),(C) Net torque input  $\tau_s$  and position error  $e_s$  of the shoulder joint, respectively. (D),(E) Net torque input  $\tau_e$  and position error  $e_e$  of the elbow joint, respectively. The movement started at 0.05s (**Algorithm 1**). (F) Average joint position error of each joint.

to zero by the end of the movement (around 0.7s), for all three whip models (Fig. 2 and 5). Damping values also showed negative or near-zero values at 0.45s. While regions with negative stiffness and damping values may compromise stability, the overall stiffness and damping resulted in positive average values, which might have prevented large deviations from the zero-torque trajectory over the course of time.

Compared to the ZTTO controller, a lower average stiffness and higher average damping values were observed for the ZTTO + OIA. This indicates that the velocity-dependent terms of the impedance controller were dominant compared to the position-dependent terms (Eq. 1). Moreover, across the whip models, a (particularly) large average stiffness and damping matrices were observed for the long whip model (Fig. 5). This could originate from higher internal stiffness and damping values of the whip model [11], [12]. We expect that a more in-depth analysis of the long whip model provides more insights into the observed high stiffness and damping values.

It is yet unclear why episodically negative stiffness and damping values were observed for the ZTTO + OIA controller. Such values could arise from the structure of the adaptation law itself (Eq. 11) — the OIA control law does

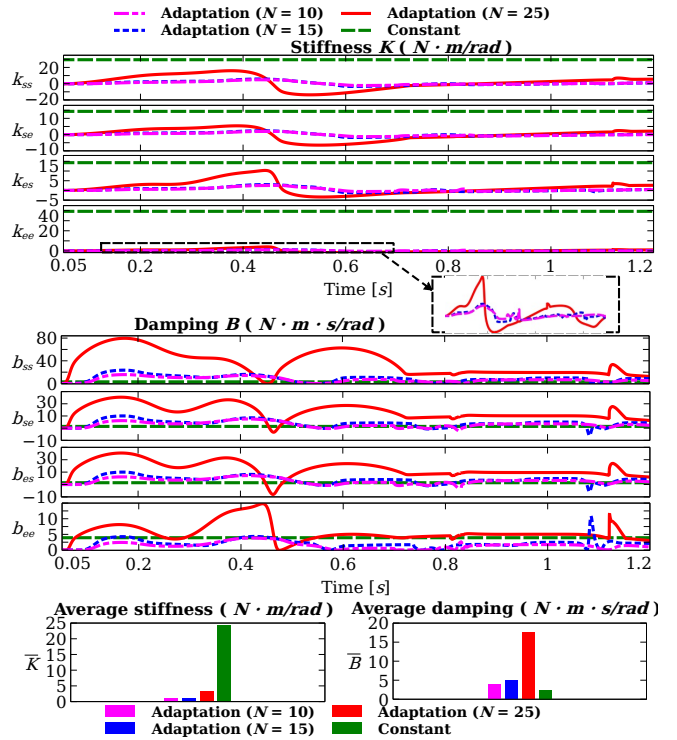


Fig. 5: Time vs. elements of impedance matrices  $K$  and  $B$  using the ZTTO + OIA controller (Eq.5). The simulation was generated by the optimal movement parameters of each whip model. The time varying impedances are compared with the constant impedance value (green) used for ZTTO controller (Eq. 13). The average stiffness  $\bar{K}$  and average damping  $\bar{B}$  (Eq. 15) for each whip model, compared with the constant impedance value (green).

not constrain the stiffness and damping values to be positive. Braun et al. suggested and validated a controller for a prosthetic leg that adapted stiffness and allowed for its negative values [15]. Such episodes occurred passively in the system. Bitz et al. suggested adaptable and negative damping for a 7-DOF robot in a human-robot interaction task [16]. Such controller resulted in reduced effort and increased accuracy. Therefore, time-varying and even negative joint stiffness and damping in the present study could facilitate exploitation of passive dynamics of the whip. In particular, when the whip and the manipulator are already moving fast enough (Fig. 2B), no additional input could be required. However, we recognize that further analysis and improvement of the overall approach may be required.

Several human studies have reported time-varying and negative joint impedances. For example, Lee et al. observed real-time modulation of the ankle impedances during walking that regulated the interaction with the ground [17]. Rouse et al. observed negative damping in the ankle joint during walking and suggested that negative damping facilitates exploitation of passive dynamics of the system [19]. Huang et al. showed the improvement of motor learning in humans when subjects were trained in a negative-viscosity force field [20].

However, to the best of our knowledge, studies which measured the time-varying impedances of the upper-limb have

not yet been conducted. Widely recognized measurements of the upper-limb impedances were done in quasi-static setups, where equilibrium could be assumed [26], [29] — rather different from the tasks with such intense movement as in manipulating a whip. Hence, for interfacing our result with biological evidence, experiments which measure the upper-limb impedances during whip manipulation remain to be conducted. Developing an experimental paradigm for such experiments is a topic of ongoing work [24].

Summarizing, this study attempted to emphasize the crucial role of varying mechanical impedance for physical interaction. The study presented a first step to combine motion primitives and interactive primitives as a control strategy that may facilitate the manipulation of objects with significant complex dynamics.

## APPENDIX

The joint stiffness matrix  $\mathbf{K} \in \mathbb{R}^{2 \times 2}$  and damping matrix  $\mathbf{B} \in \mathbb{R}^{2 \times 2}$  used for the ZTTO controller are given by [11]:

$$\mathbf{K} = \begin{bmatrix} 29.5 & 14.3 \\ 14.3 & 39.3 \end{bmatrix}, \quad \mathbf{B} = 0.1\mathbf{K} = \begin{bmatrix} 2.95 & 1.43 \\ 1.43 & 3.93 \end{bmatrix} \quad (13)$$

The average values of the joint stiffness  $\bar{\mathbf{K}}$  and damping matrices  $\bar{\mathbf{B}}$  are calculated as follows:

$$\bar{\mathbf{K}} = \frac{1}{4} \sum_{i=0}^3 \left( \frac{\sum_{j=0}^N |\text{vec}(\mathbf{K})_i(t_0 + j \cdot \Delta T)|}{N} \right), \quad (14)$$

$$\bar{\mathbf{B}} = \frac{1}{4} \sum_{i=0}^3 \left( \frac{\sum_{j=0}^N |\text{vec}(\mathbf{B})_i(t_0 + j \cdot \Delta T)|}{N} \right) \quad (15)$$

where  $t_0 = 0.05\text{s}$  is the time when the movement starts,  $\Delta = 0.1\text{ms}$  is the time step of the simulation and  $N$  is the number of samples collected from start to end of zero-torque trajectory with duration  $D$ , i.e.,  $N = D/\Delta T$ .

## ACKNOWLEDGMENT

The authors would like to thank Anders Lyhne Christensen for support and consulting during this work.

## REFERENCES

- [1] A. Billard and D. Kragic, “Trends and challenges in robot manipulation,” *Science*, vol. 364, no. 6446, 2019.
- [2] O. M. Andrychowicz, B. Baker, M. Chociej, R. Jozefowicz, B. McGrew, J. Pachocki, A. Petron, M. Plappert, G. Powell, A. Ray, et al., “Learning dexterous in-hand manipulation,” *The International Journal of Robotics Research*, vol. 39, no. 1, pp. 3–20, 2020.
- [3] R. E. Bellman, *Adaptive control processes: a guided tour*, vol. 2045. Princeton university press, 2015.
- [4] N. Hogan and D. Sternad, “Dynamic primitives of motor behavior,” *Biological Cybernetics*, vol. 106, no. 11, pp. 727–739, 2012.
- [5] N. Hogan, “Physical Interaction via Dynamic Primitives,” in *Geometric and Numerical Foundations of Movements* (J.-P. Laumond, N. Mansard, and J.-B. Lasserre, eds.), pp. 269–299, Cham: Springer International Publishing, 2017.
- [6] H. Guang, S. Bazzi, D. Sternad, and N. Hogan, “Dynamic primitives in human manipulation of non-rigid objects,” in *2019 International Conference on Robotics and Automation (ICRA)*, pp. 3783–3789, IEEE, 2019.
- [7] B. Nasseroleslami, C. J. Hasson, and D. Sternad, “Rhythmic manipulation of objects with complex dynamics: predictability over chaos,” *PLoS Comput Biol*, vol. 10, no. 10, p. e1003900, 2014.
- [8] R. Nayeem, S. Bazzi, N. Hogan, and D. Sternad, “Transient Behavior and Predictability in Manipulating Complex Objects,” in *2020 IEEE International Conference on Robotics and Automation (ICRA)*, pp. 10155–10161, may 2020.
- [9] S. Bazzi and D. Sternad, “Robustness in human manipulation of dynamically complex objects through control contraction metrics,” *IEEE Robotics and Automation Letters*, vol. 5, no. 2, pp. 2578–2585, 2020.
- [10] S. Schaal, “Dynamic Movement Primitives - A Framework for Motor Control in Humans and Humanoid Robotics,” in *Adaptive Motion of Animals and Machines* (H. Kimura, K. Tsuchiya, A. Ishiguro, and H. Witte, eds.), pp. 261–280, Tokyo: Springer-Verlag, 2006.
- [11] M. C. Nah, A. Krotov, M. Russo, D. Sternad, and N. Hogan, “Dynamic Primitives Facilitate Manipulating a Whip,” in *2020 8th IEEE RAS/EMBS International Conference for Biomedical Robotics and Biomechatronics (BioRob)*, pp. 685–691, nov 2020.
- [12] M. C. Nah, *Dynamic primitives facilitate manipulating a whip*. Master of science thesis, Massachusetts Institute of Technology, 2020.
- [13] B. Bernstein, D. A. Hall, and H. M. Trent, “On the dynamics of a bull whip,” *The Journal of the Acoustical Society of America*, vol. 30, no. 12, pp. 1112–1115, 1958.
- [14] G. Averta and N. Hogan, “Enhancing robot-environment physical interaction via optimal impedance profiles,” in *2020 8th IEEE RAS/EMBS International Conference for Biomedical Robotics and Biomechatronics (BioRob)*, pp. 973–980, IEEE, 2020.
- [15] D. J. Braun, V. Chalvet, and A. Dahiya, “Positive-Negative Stiffness Actuators,” *IEEE Transactions on Robotics*, vol. 35, pp. 162–173, Feb 2019.
- [16] T. Bitz, F. Zahedi, and H. Lee, “Variable Damping Control of a Robotic Arm to Improve Trade-off between Agility and Stability and Reduce User Effort,” in *IEEE International Conference on Robotics and Automation*, pp. 11259–11265, Institute of Electrical and Electronics Engineers Inc., May 2020.
- [17] H. Lee and N. Hogan, “Time-varying ankle mechanical impedance during human locomotion,” *IEEE Transactions on Neural Systems and Rehabilitation Engineering*, vol. 23, no. 5, pp. 755–764, 2014.
- [18] F. Lacquaniti, M. Carrozzo, and N. A. Borghese, “Time-Varying Mechanical Behavior of Multijointed Arm in Man,” *Journal of Neurophysiology*, vol. 69, no. 5, pp. 1443–1463, 1993.
- [19] E. J. Rouse, L. J. Hargrove, E. J. Perreault, and T. A. Kuiken, “Estimation of human ankle impedance during the stance phase of walking,” in *IEEE Transactions on Neural Systems and Rehabilitation Engineering*, pp. 870–878, Institute of Electrical and Electronics Engineers Inc., 2014.
- [20] F. C. Huang, J. L. Patton, and F. A. Mussa-Ivaldi, “Manual Skill Generalization Enhanced by Negative Viscosity,” *Journal of Neurophysiology*, vol. 104, pp. 2008–2019, oct 2010.
- [21] X. Xiong and P. Manoonpong, “Adaptive Motor Control for Human-like Spatial-temporal Adaptation,” in *IEEE International Conference on Robotics and Biomimetics*, (Kuala Lumpur), pp. 2107–2112, 2018.
- [22] E. Todorov, T. Erez, and Y. Tassa, “MuJoCo: A physics engine for model-based control,” in *2012 IEEE/RSJ International Conference on Intelligent Robots and Systems*, pp. 5026–5033, oct 2012.
- [23] H. Hatze, “A mathematical model for the computational determination of parameter values of anthropomorphic segments,” *Journal of Biomechanics*, vol. 13, no. 10, pp. 833–843, 1980.
- [24] A. Krotov, *Human Control of a Flexible Object: Hitting a Target with a Bull-Whip*. Master of science thesis, Northeastern University, 2020.
- [25] T. Flash and N. Hogan, “The coordination of arm movements: an experimentally confirmed mathematical model,” *Journal of neuroscience*, vol. 5, no. 7, pp. 1688–1703, 1985.
- [26] J. McIntyre, F. A. Mussa-Ivaldi, and E. Bizzi, “The control of stable postures in the multijoint arm,” *Experimental Brain Research*, vol. 110, no. 2, pp. 248–264, 1996.
- [27] J.-J. E. Slotine, “Sliding controller design for non-linear systems,” *International Journal of control*, vol. 40, no. 2, pp. 421–434, 1984.
- [28] J. M. Gablonsky and C. T. Kelley, “A Locally-Biased form of the DIRECT Algorithm,” *Journal of Global Optimization*, vol. 21, no. 1, pp. 27–37, 2001.
- [29] F. Mussa-Ivaldi, N. Hogan, and E. Bizzi, “Neural, mechanical, and geometric factors subserving arm posture in humans,” *The Journal of Neuroscience*, vol. 5, pp. 2732–2743, oct 1985.